Earthquakes and Structures, *Vol. 18, No. 5 (2020)637-648*
DOI: https://doi.org/10.12989/eas.2020.18.5.637

Numerical and experimental study of the nested-eccentric-cylindrical shells damper

Alireza Reisi*[1], Hamid Reza Mirdamadi[2] and Mohammad Ali Rahgozar[3]

[1]*Department of Civil Engineering, Isfahan (Khorasgan) Branch, Islamic Azad University, Isfahan, Iran*
[2]*Department of Mechanical Engineering, Isfahan University of Technology, Isfahan, Iran*
[3]*Department of Civil Engineering and Transportation, University of Isfahan, Isfahan, Iran*

(*Received September 16, 2019, Revised December 16, 2019, Accepted December 26, 2019*)

Abstract. In this study, a new steel cylindrical shell configuration of the dissipative energy device is proposed to improve lateral ductility and to reduce the damage of the structures against seismic forces. Four nested-eccentric- cylindrical shells are used to constructing this device; therefore, this proposed device is named nested-eccentric-cylindrical shells damper (NECSD). The particular configuration of the nested-eccentric-cylindrical shells is applied to promote the mechanical characteristics, stability, and overall performance of the damper in cyclic loads. Shell-type components are performed as a combination of series and parallel non-linear springs into the in-plan plastic deformation. Numerical analysis with respect to dimensional variables are used to calculate the mechanical characteristics of the NECSD, and full-scale testing is conducted for verifying the numerical results. The parametric study shows the NECSD with thin shells were more flexible, while devices with thick shells were more capacious. The results from numerical and experimental studies indicate that the NECSD has a stable behavior in hysteretic loops with highly ductile performance, and can provide appropriate dissipated energy under cyclic loads.

Keywords: dampers; energy dissipation; finite element method; hysteretic damper; structural control

1. Introduction

One of the significant challenges facing structural engineers is the adoption of advanced methods in increasing the safety and stability of the structures against earthquake. In traditional manners, all members of structures are designed to resist within elastic range for lateral excitations. Consequently, in new approaches, the basic members provide stability with maximum strength, while the non-basic members provide plastic deformations without collapse (Priestley *et al*. 2007, Plevris *et al.* 2017). In this context, some devices are introduced as members to dissipate seismic energy and to control the dynamic behavior of the structure. Applying these particular devices lead to the development of the concept of 'control' in structures.

Passive control devices, including dampers, have advanced in the past three decades. Dampers dissipate seismic energy through a variety of mechanisms, such as friction, yield, viscose, and viscoelastic. The function of the friction and yield dampers is dependent on the displacement, while the performance of viscose and viscoelastic types are related to the velocity or combination of displacement and velocity. Many studies exist on yield mechanisms for dissipating seismic energy devices based on applying ductile materials for the dampers with displacement function. Yield dampers, the subject of this article, are cost-effective, easy to install, replaceable after the earthquake and have an appropriate function in dissipating seismic energy. The most common metal applied in 'yield damper' is of mild steel; however, in some cases lead or other types of metal are applied (Soong and Dargush 1997, Soong and Spencer Jr 2002, Liang *et al.* 2011, Castaldo 2014)

The most popular devices in the field of yield damper consist of Added Damping and Stiffness (ADAS) and advanced (TADAS); Triangular-plate ADAS dampers. They come in shapes of an hourglass and triangular (Bergman and Goel 1987, Tsai *et al.* 1993). Both these dampers can be attached to the top of an inverted-V brace frame to dissipate seismic energy.

Suzuki and Watanabe (2000) proposed U-shaped damper. This device is made of two U-shaped steel plates to dissipate seismic energy for higher performance in the out-of-plane plastic deformation. Shape optimization of U-shaped damper for improving its bi-directional performance under cyclic loading is assessed by Deng *et al.* (2015).

The prominent of the other types of yield dampers with shear deformation performance are shear-wall panel and slit dampers. These devices are made of steel plates for performing in the in-plane shear deformation. For the first time, Nakagawa *et al.* (1996), introduced steel shear-wall panel as a dissipating energy device. The performance of low-yield-strength steel shear-panel damper with without buckling are investigated by Zhang *et al.* (2015). Ricky and Faris (2008) proposed slit damper, Tagawa *et al.* (2016) focused on cyclic behavior of this type damper and Kim *et al.* (2017) considered on optimal distribution slit damper for seismic retrofit of structures. The main structure of the dampers described above is based on the plate; recently, in

*Corresponding author, Ph.D. Student
E-mail: alireza.reisi@khuisf.ac.ir

http://www.techno-press.com/journals/was&subpage=7
ISSN: 2092-7614 (Print), 2092-7622 (Online)

order to enhance the performance of metal components in yield dampers, some efforts carried out to apply cylindrical shell structure in damper configuration; accordingly, the samples of pipe-shaped dampers are introduced. A cylindrical shell configuration device, called 'pipe-damper' (PD) is assessed, tested, and confirmed by Maleki and Bagheri (2010). Dual-pipe damper (DPD) with adding a pipe on the one side of the PD, is introduced by Maleki and Mahjoubi (2013), which increases the stiffness and damping of the device compared to the previous one. Although these two dampers are developed to apply cylindrical shell in the structure of damper, their lacks are low redundancy to failure and act merely in shear deformation.

Applying two or multi-level control systems is one of the new methods which has become an interesting issue among researchers in recent years. By applying this concept, (Cheraghi and Zahrai 2016, Zahrai and Cheraghi 2017) developed a new type of pipe damper, which consists of a number of nested concentric pipes connected together by some pistons. A gap exists between pipes due to the flexural stiffness of the outer pipe consider to their lengths, diameters, and thicknesses. The manufacturing and installation of this damper are complicated, but its function is increased in comparison with the two previous cylindrical shell-type dampers.

Considering that the cylindrical shell structure is more capacious versus the plate, the focus of this study is on dampers, which are designed based on cylindrical shell structural components. However, the previously proposed devices with cylindrical shell structure are not perfect because the shell components in these devices are subject to either shear or axial behaviors and they also have a single-load path failing mechanism in loading presses, which means, if a component fails in loading, the functionality of the system is stopped completely.

Accordingly, in this study, a new configuration of the cylindrical shell structure is proposed for the passive energy dissipation device with some components by a combination of both shear and axial behaviors. In this device, four nested eccentric cylindrical shell acts as a non-linear spring by a combination of series and parallel form, that means, if a component fails during a loading process, the overall function of the system will not be disrupted completely, and it can act continue with a lower capacity. Besides, the seismic force from the brace is directly carried by this device without the need to decompose it into the horizontal and vertical components (such as ADAS, TADAS, etc.). In this research, mechanical characteristics of the proposed damper are calculated by numerical models, and two full-scale prototypes are manufactured and tested for verifying the numerical results. Finally, some of the results of the mechanical characteristics are discussed in the parametric study section.

2. Configuration of nested-eccentric-cylindrical shells damper

The nested-eccentric-shells damper (NECSD), as shown in Fig. 1, is constructed with four cylindrical shells (or

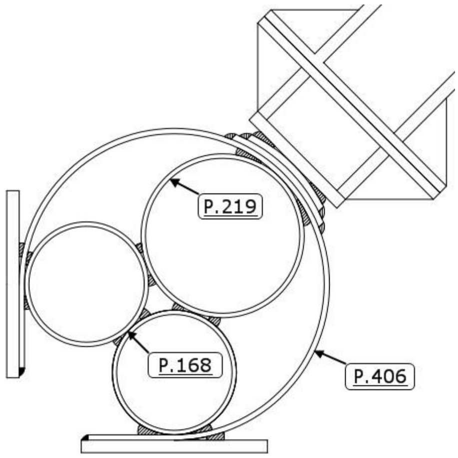

Fig. 1 Nested-eccentric-cylindrical shells damper

pipes), with 406, 219, and 168 mm diameter and length of 150 mm. All diameters of the pipes correspond to that of APL 5L (2000) standard. According to the standard fixed size of the pipes in the market, the diameter of the outer cylindrical shell is selected based on the geometric limitation fit to cover the inner cylindrical shells, and the diameter of the inner cylindrical shells are chosen based on the geometric limitation fit to embed in the outer cylindrical shell. Although there is a limitation to selecting the diameter of pipes in the configuration of the NECSD, a wide range of capacity would become possible by changing the thickness of the outer and inner cylindrical shells. Consequently, the diameter and the length of cylindrical shells are fixed, and only the shell thickness is considered as a design variable.

The cylindrical shells are connected to one another by conventional welding but to enhance the plastic performance and reduce the damaging effects due to welding, it is recommended to manufacture these components by advanced welding methods or casting metal process.

The cylindrical shells are applied in the configuration of the NECSD act as non-linear springs in series and parallel form. The outer cylindrical shell, P. 406 is a circumscriber and main member of the device that transmits tensile and compressive forces to the inner cylindrical shells. The placement of inner cylindrical shells nested into the outer cylindrical shell will promote the mechanical strength and stability in the structure of the damper. The two cylindrical shells together, P.168, made a combination of parallel springs in the bearing part of the device. However, P.219 is as a series spring with the equivalent spring of the two previous members (P.168). The outer cylindrical shell, P.406 also is in a parallel form with the equivalent spring formed by a combination of P.219 and two P.168 pipes. As mentioned, it indicates how each member could transmit load in a single load path to another load path. The safety is considered in the configuration of the NECSD because if any of the members fail during loading, the other members would act to continue the performance, thus, the operation of the device would not stop suddenly.

The deferent types of NECSD installations in diagonal and/or inverted-V braced frames at the connection of beams

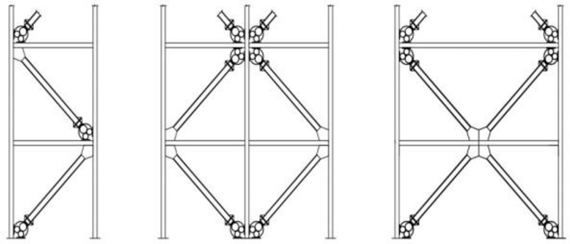

Fig. 2 Schematic of NECSD installations in diagonal and/or inverted-V braced frames

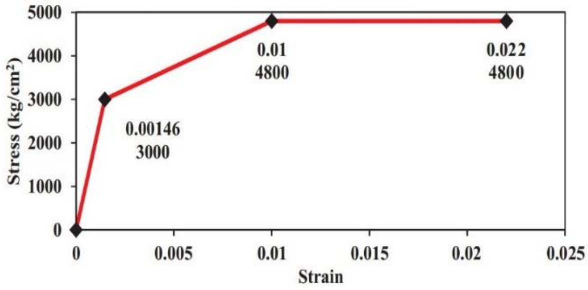

Fig. 3 Stress-strain diagram defined in the software for CT20 Steel (Andalib et al. 2018)

and columns without gusset plates are shown in Fig. 2. To avoid any change in the perpendicular angle at the bearings of the device, it is recommended to apply rigid moment connections for beam to column.

2.1 Stability of the device

Based on the theory of plates and shells, the buckling of cylindrical shells with a short, intermediate, and long length under the exterior pressure is confirmed by Ventsel and Krauthammer (2001). The cylindrical shell with long-length is not applicable in this study; Moreover, the cylindrical shell with an intermediate-length is more stable than the cylindrical shell with short-length. Therefore, the length and diameter of the cylindrical shells in the NECSD are chosen in the range of the cylindrical shell with intermediate-length. The critical value of the uniform external pressure, P_{cr}, to control the stability of the cylindrical shell with intermediate-length when $0.3\ \sqrt{R/t}\ > L/R\ > \sqrt{t/R}$, is calculated by Eq. (1)

$$P_{cr} = 0.92\frac{Et^2}{RL}\sqrt{\frac{t}{R}} \tag{1}$$

where, L, t, R, and E are the length (depth of cross-section), thickness of the shell, radius of the shell from center point, and modulus of elasticity, respectively. However, the buckling capacity of the cylindrical shell is reduced by an increase in the radius and length and/or a decrease in thickness. Due to the fixed-length (150 mm) of all members and also their varying radius and thickness, the critical member for stability analysis should be P.406. This member meets the condition of the length-to-radius ratio with its largest radius for intermediate-length cylindrical shells. It is a conservative assumption for stability control if the P_{cr} value corresponding to thickness of P.406 is greater than the yield force from FEA models. Therefore, the stability of the device is controlled by the mentioned approach. Besides, based on the effect of a partial load (on the part of surface) versus uniform load on all around of cylindrical shell (Vodenitcharova and Ansourian 1998), the cylindrical shell under a partial load is more stable than the cylindrical shell under a uniform load. Moreover, it will be observed in experimental tests and numerical models, that the configuration of the nested eccentric cylindrical shells can increase the overall stability for the device.

3. Numerical simulation

The Finite Element Analysis (FEA) is the simulation of any given physical phenomenon using the numerical technique called Finite Element Method (FEM). FEM is used to find the solution to the forces, deformations, etc., by minimizing the potential energy of the system under the applied loads. Engineers use it to reduce the number of physical prototypes and experiments and optimize components in their design phase to develop better products, faster.

To assess the performance and mechanical behavior of this proposed damper, Finite Element (FE) simulation models of NECSD are analyzed by a three-dimensional finite element analysis software called ABAQUS package (version 6.13-1, 2013) to evaluate the hysteresis characteristics and low cycle behavior.

3.1 Materials applied in the analyses

Most metal pipes construct by carbon steel materials. The CT20 steel is an available type of carbon steel metal for pipes that it is specified in GOST Specification 8733 (1976). The pipes used in NECSD are of this type of metal. The tri-linear stress-strain curve, including hardening material behavior, as shown in Fig. 3, is proposed by Andalib *et al.* (2018) for the CT20 materials. Based on this reference, this tri-linear stress-strain curve could be assigned for the material of the FE models, and the numerical data are modified slightly by experimental data to obtain a better fit result between the experimental and numerical data.

3.2 Non-linear finite element analysis

Finite element analyses (FEA) are run on 3D static non-linear models. Different thicknesses of cylindrical shells as a variable are applied in numerical NECSD models, and the type of property is assigned 'shell' for all elements on NECSDs with large deformation effects. 'S4R' element with isotropic hardening, reduced integration, and hourglass control is applied for modeling the cylindrical shells. The S4R element is defined by four nodes with double curved thin or thick shell appropriate for a wide range of applications expanded into the 3D element.

Table 1 Thicknesses of NECSD samples

Sample	Thickness [mm]		
	P.168	P.219	P.406
NECSD.1	6.4	6.4	6.4
NECSD.2	6.4	6.4	10.3
NECSD.3	6.4	6.4	14.3
NECSD.4	8.7	8.7	7.1
NECSD.5	8.7	8.7	11.1
NECSD.6	8.7	8.7	15.9
NECSD.7	11.1	11.1	8.7
NECSD.8	11.1	11.1	11.9
NECSD.9	11.1	11.1	17.5
NECSD.10	6.4	6.4	9.5
NECSD.11	8.7	8.7	12.7
NECSD.12	11.1	11.1	19.1

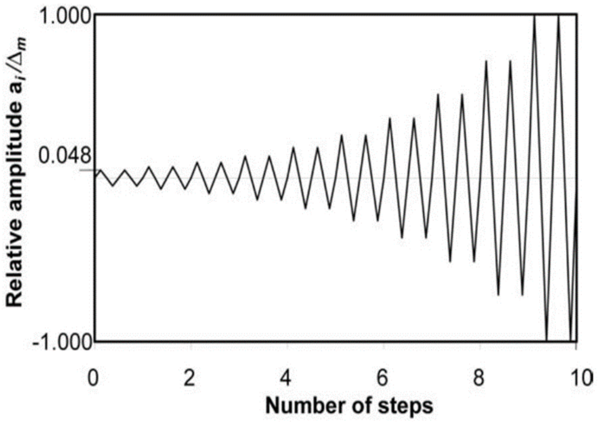

Fig. 4 Loading protocol for a1 =0.048 Δm (FEMA 461)

To assess the mechanical characteristics of NECSD, the details of twelve models with different thickness variation are tabulated in Table 1. With respect to the high effect of P.406 on the mechanical characteristics of the modeled device, all different available thicknesses in the market are selected for this pipe in FE models.

Non-linear FEAs are run on models with 10-step dual peak loads, (i.e., 20 cycles of loading) concerning FEMA 461 loading protocol. The amplitudes of the loading protocol are shown in Fig. 4. The following equation expresses the amplitudes $a_{i+1}$of the step $i+1$ (each step has two cycles)

$$a_{i+1} = 1.4\ a_i \tag{2}$$

where, a_i is the amplitude of the preceding step, and a_{i+1} increases gradually up to the target displacement, Δ_m. To determine the mechanical properties in FE simulation, the models are analyzed by an approximate plastic deformation for the first time, then each model is reloaded and analyzed according to the mentioned loading protocol again. This procedure has been repeated several times to obtain constant mechanical properties results for each model. In FE simulation, the top of contact P.406 to brace is subject to cyclic load and the boundary condition is fixed at the contact P.406 to beam and column. The stress contour on the elements and deformed shapes of a FE model are shown in Fig. 5.

3.3 FEA results

Hysteretic loops show the dependence of the state of a system on its behavior in the loading procedure. The values of a force-displacement are used often to plot a loop or hysteresis curve, where there are different values of one variable depending on the direction of change of another variable. The method of drawing the force-displacement curve based on hysteretic loops is shown in Fig. 6. The force-displacement curves for these twelve models up to the maximum plastic deformation are shown in Fig. 7. According to assumed loading direction in FE simulation, the pressure with positive signs and tensile with negative signs are marked.

The hysteretic loops in the most experimental and numerical studies, that the structure by cylindrical shells used in its structure, have an asymmetric shape (Abbasnia *et al*. 2008). Therefore, as expected, the shape of the hysteretic loops in the FE models has also an asymmetric shape; thus, this expression is considered in Fig. 8 by some parameters like tensile overstrength: 'n', second stiffness factor at pressure: 'sc' and second stiffness factor for tensile: 'st'. The other mechanical parameters of non-linear FEA of the models in hysteretic loops are drawn in Fig. 8. The mechanical characteristics of each model such as yield force: 'Qy', ultimate force: 'Qu', capacity of yield/ultimate force: 'm', elastic stiffness: 'Ke', and effective stiffness: 'Keff' are tabulated in Table 2.

In this study, the maximum plastic deformation: 'Dt', as recommended in ATC-24 Standard, is considered five times the yield displacement: 'δy' and it is considered equal to the target displacement 'Δ_m' in cyclic loading protocol. This limitation by a conservative approach is assumed just for calculating mechanical characteristics for FEA in hysteretic loops, although, the physical full-scale of the proposed damper could have displacement capacity more than this assumed value. The effective stiffness: 'Keff', as suggested in FEMA 356 (2000), calculated by Eq. (3) at the maximum displacement.

$$K_{eff} = \frac{|F+| + |F-|}{|D+| + |D-|} \tag{3}$$

where, the ultimate forces: F+ = +Qu and F– = -Qu, are at the ultimate displacements of D+ = +Dt and D– = -Dt on the loading cycle, respectively.

According to the average value for 'n' parameter in Table 2, the tensile strength of the damper is about 20% greater than the compressive strength, while the compressive strength is propounded for parametric study in a conservative manner. As shown in Table 2, the S_r value is a ratio of effective stiffness/elastic stiffness. In FEA, it is observed the hysteretic loops with $0.30 \le S_r \le 0.35$ could have an appropriate shape.

One of the essential parameters considered in energy dissipation devices is the viscous damping ratio. This amount should be justifying an energy dissipation device to apply in the structures. The equivalent viscous damping ratio of the hysteretic dampers is calculated by following Eq. (Chopra 1995).

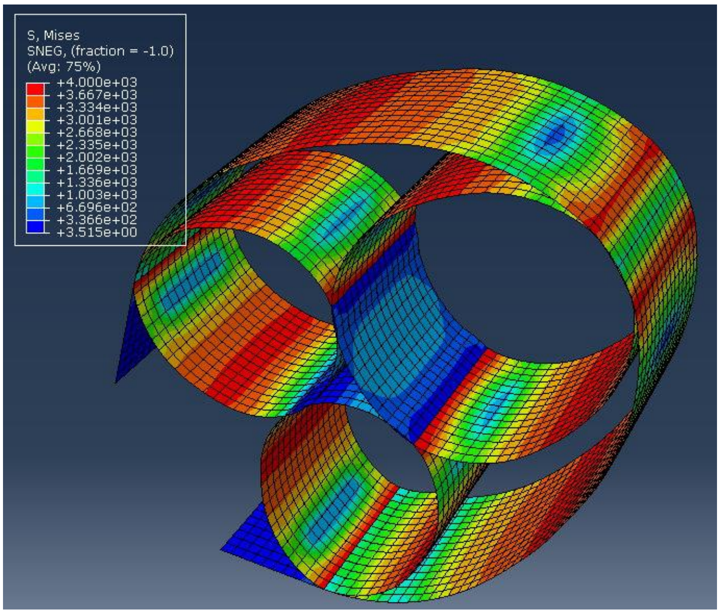

(a) Tensile contour

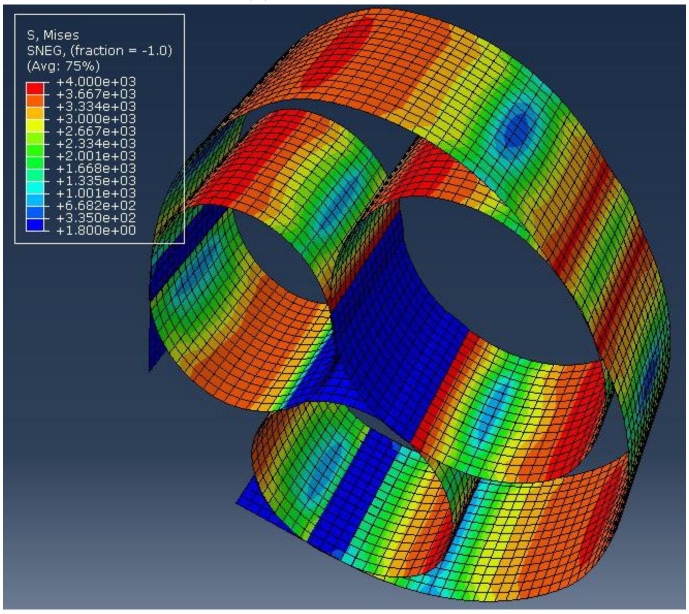

(b) Pressure contour

Fig. 5 Stress contours and deformed shapes for NECSD.1 in (a) tensile and (b) pressure

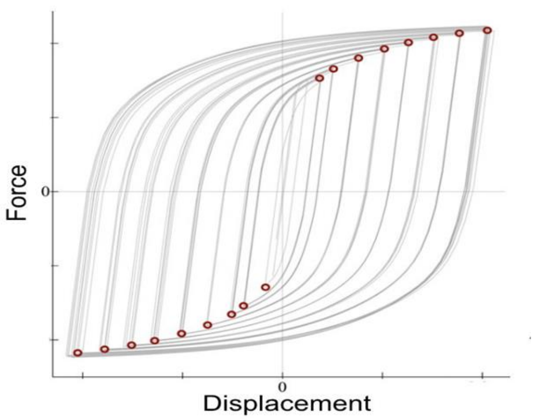

Fig. 6 The method of draw load-displacement curves from hysteretic loops

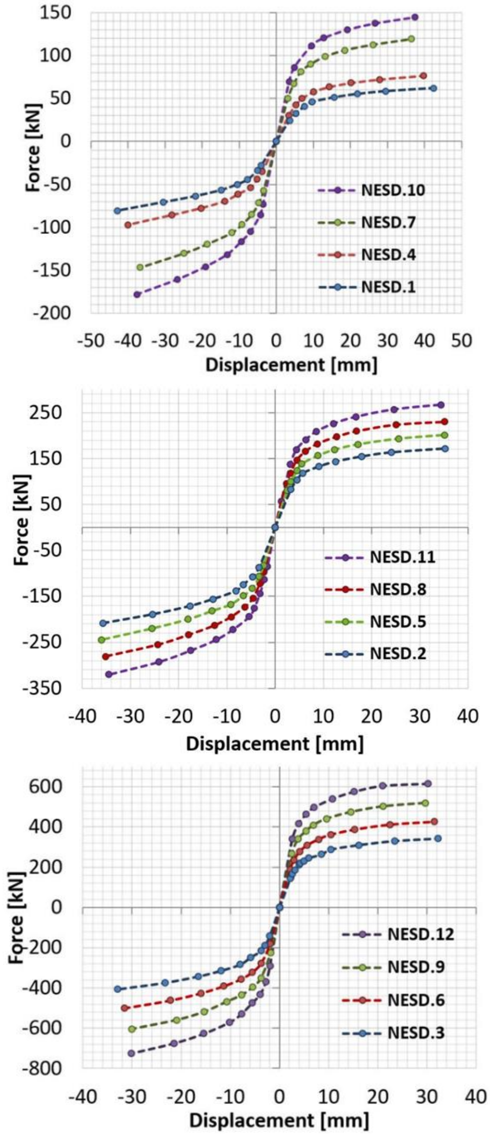

Fig. 7 The force-displacement curves form hysteretic loops for “NECSDs” in FEA models

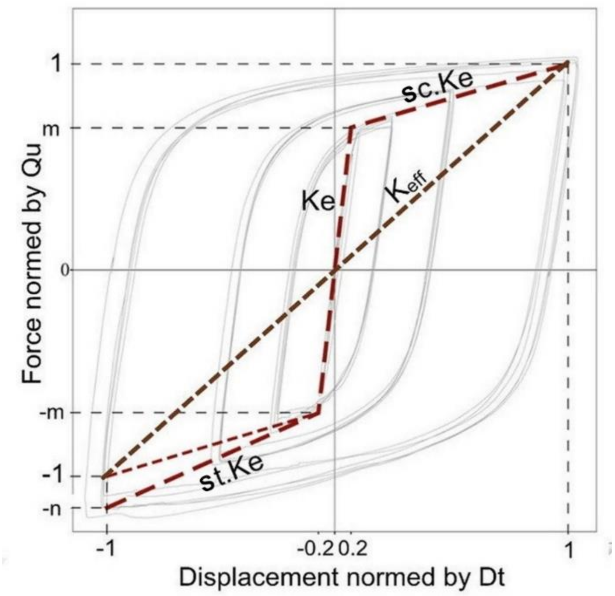

Fig. 8 Mechanical parameters from theoretical bilinear curve

Table 2 Calculated mechanical parameters for NECSD models

Sample	Q_y [kN]	m	Q_u [kN]	n	δ_y [mm]	D_t [mm]	K_e [kN/mm]	sc	st	K_{eff} [kN/mm]	Sr = K_{eff} /K_e
NECSD.1	39.20	0.63	62.07	1.30	8.6	42.9	4.56	0.15	0.27	1.62	0.35
NECSD.2	108.80	0.64	171.35	1.22	7.2	35.8	15.21	0.14	0.23	5.16	0.34
NECSD.3	231.47	0.68	342.21	1.19	6.6	32.9	35.15	0.12	0.19	11.00	0.31
NECSD.4	47.69	0.62	76.43	1.27	8.0	40.0	5.95	0.15	0.26	2.09	0.35
NECSD.5	132.05	0.66	201.03	1.22	7.2	36.1	18.30	0.13	0.21	5.99	0.33
NECSD.6	285.40	0.67	425.69	1.18	6.3	31.5	45.25	0.12	0.19	14.25	0.31
NECSD.7	74.79	0.63	119.02	1.23	7.4	36.8	10.17	0.15	0.24	3.49	0.34
NECSD.8	153.43	0.67	229.80	1.22	7.0	35.2	21.82	0.12	0.21	7.06	0.32
NECSD.9	348.82	0.67	519.27	1.16	6.1	30.4	57.29	0.12	0.18	18.23	0.32
NECSD.10	92.76	0.65	141.82	1.24	7.3	36.5	12.71	0.14	0.23	4.20	0.33
NECSD.11	182.44	0.66	276.84	1.19	6.7	33.5	27.23	0.13	0.20	8.71	0.32
NECSD.12	412.05	0.67	615.40	1.18	6.0	30.2	68.13	0.12	0.19	21.64	0.32

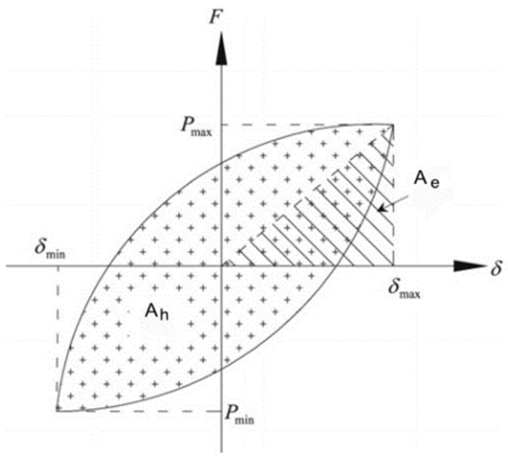

Fig. 9 The force-displacement diagram to calculate the equivalent viscous damping ratio (Chopra, 1995)

Table 3 Equivalent viscous damping ratios of the NECSD samples

Sample	A_h [J]	A_e [J]	A_h/ A_e	ξ_{eq}
NECSD.1	7034.4	1318.1	5.34	0.42
NECSD.2	16447.1	3024.7	5.44	0.43
NECSD.3	31612.3	5519.7	5.73	0.46
NECSD.4	8023.3	1518.2	5.28	0.42
NECSD.5	19399.7	3535.1	5.49	0.44
NECSD.6	36351.5	6702.1	5.42	0.43
NECSD.7	11621.7	2167.8	5.36	0.43
NECSD.8	22282.4	4066.1	5.48	0.44
NECSD.9	41716.8	7691.8	5.42	0.43
NECSD.10	14131.5	2588.2	5.46	0.43
NECSD.11	25411.1	4637.1	5.48	0.44
NECSD.12	53008.2	9404.5	5.64	0.45
Average			5.46	0.43

$$\xi_{eq} = \frac{A_h}{4\pi A_e} \tag{4}$$

As observed in Fig. 9, A_h and A_e are the dissipated energy in a loading cycle and the amount of energy stored in a non- linear device, respectively.

The values of the equivalent viscous damping according to hysteretic loops for NECSD models are tabulated in Table 3. The sum of negative and positive projection parts of a hysteretic loop on the horizontal axis is ten times of yield displacement. As observed in Table 3, the average value equivalent viscous damping is about 43% for the models of concern. It is a desirable value for an energy dissipation device without resorting to the complicated and expensive energy dissipation device.

4. Experimental discussion

As previously stated, simulated numerical models are used to evaluate the mechanical characteristics and behavior of engineering structures. In engineering works, if the number and size of the models are limited, to verify the numerical models, used a number of full-scale samples equal to a number of the numerical models. Otherwise, by reducing the number of full-scale prototypes, could be verifying a limited number of numerical models with the full-scale samples and transmit the findings of this verification to other numerical models. Accordingly, the two full-scale prototypes are built according to the dimensions of the two FE models and verifying the FE models by the manner described above.

4.1 Specimens and test setup

The purpose of the full-scale test is to assess, compare, and verify the numerical results with a minimum of two full-scale models. The experimental specimens are constructed based on the dimension of NECSD.1 and NECSD.2 in the FE models. The specimens and the placement on the loading actuator machine are shown in Figs. 10 and 11.

The damper components are connected by the shielded metal arc welding (SMAW) by E60 electrode. A pass-through groove with 6 mm effective throat welded to both sides of the connection. To enhance the performance of the device, advanced welding methods or casting metal techniques are recommended in damper construction.

Fig. 10 Two full-scale specimens

Fig. 11 Test setup of NECSD

The specimens are setup into the SANTAM (STM-400) actuator machine with a capacity of 1000 kN. To simulate the connection of the damper to the frame at the structure, an L-shaped fixture is used at the bottom of the actuator machine. The displacement and load are measured by the sensor of the actuator machine that calibrated before the test.

4.2 Experimental verification

The tests are run according to displacement-controlled method and the cyclic loads which gradually increase due to the above-mentioned load testing protocol. After running loading protocol for the NECSD.1 sample, the P.219 cylindrical shell tolerates up to the 75% of the total loading capacity and fails at the 15th loading cycle, while the P.406 cylindrical shell tolerated up to the 85% of the full loading capacity and fails at the 17th loading cycle, which is measured 30.6 mm. The fracture in the cylindrical shells, as shown in Fig. 12, occurred close to the welded zone. The major cause of these fractures is the harmful effects in the welded zone.

The specimen NECSD.2 tolerated more than 100 % of total loading capacity at 22nd loading cycle. The maximum plastic deformation, Dt, is estimated as 35.8 mm at 20th loading cycle for this specimen. The extra plastic deformation is chosen as Dt+5 mm at 21st and 22nd loading cycle. Fracture in this sample occurred simultaneously at P.406 and P.219 at 22nd loading cycle close to the welding zone. Maximum compressive and tensile deformations at 19th and 20th loading cycles are shown in Fig. 13.

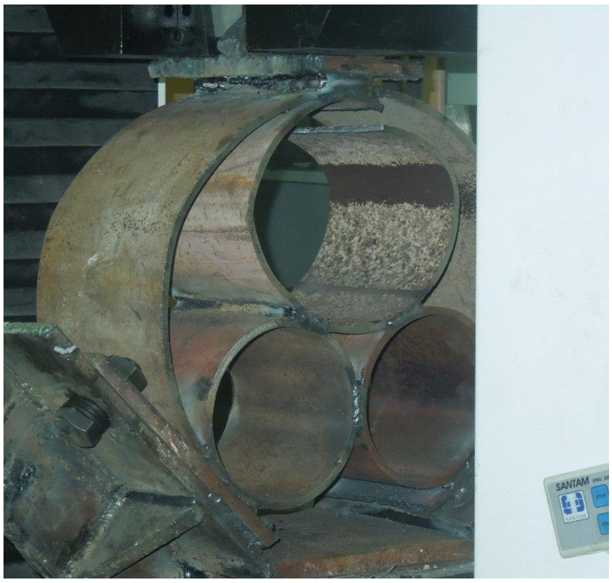

Fig. 12 NECSD.1 specimen after failure on P.219 at 15th cycle

Table 4

Data comparing for experimental /numerical ratio

Sample	Number of cycle	Qy	δy	Ke	Qu	Dt	Keff
NECSD.1	0.85	0.97	1.02	0.96	0.81	0.76	N/A
NECSD.2	1.10	0.98	1.01	0.98	1.08	1.12	0.98

Hysteretic loops of specimens in the form of numerical analyses and the test results are shown in Fig. 14. By comparing the numerical and experimental results in Fig. 14(a), a difference is observed in the last loading cycles. This difference, as shown in Fig .12 for NECSD.1, due to the fracture of P.219 in the welding zone through the cyclic loading. The harmful effects in the welded zone at the connection of the pipes should be considered as a significant limitation in reducing the displacement capability for manufacturing proposed damper. This deficiently in the welded zone could be solved by manufacturing dampers with advanced welding methods or casting metal process. This fracture is important if it occurs in the plastic hinge at the middle of the cylindrical shell length. However, for this sample, the laboratory data are applied only for verifying the numerical data before occurring the fracture at the member of the specimen. As shown in Fig. 14(b), a good matching exists between the experimental and FEA hysteretic loops for NECSD.2. The results of full-scale tests are applied in verifying the two numerical models and this verification is applied in the other numerical models.

The hysteretic loops of specimens indicate a more capacity by a gentle slope within non-linear tensile

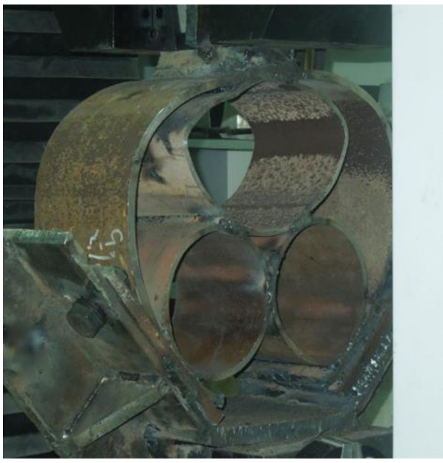

(a) at 19th loading cycle

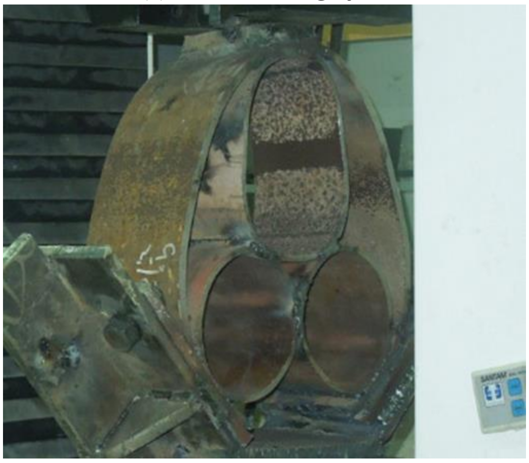

(b) at 20th loading cycle

Fig. 13 Maximum displacement of NECSD.2

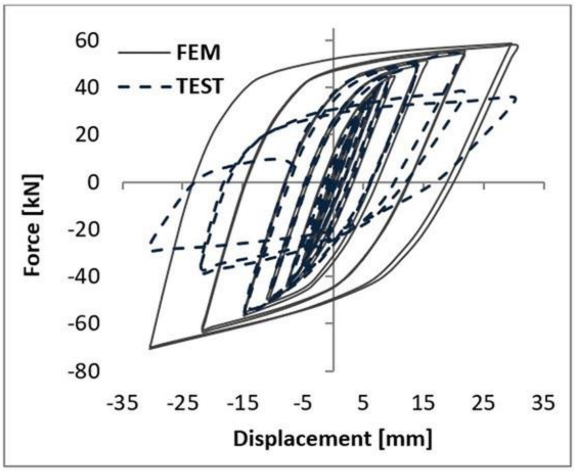

(a) NECSD.1

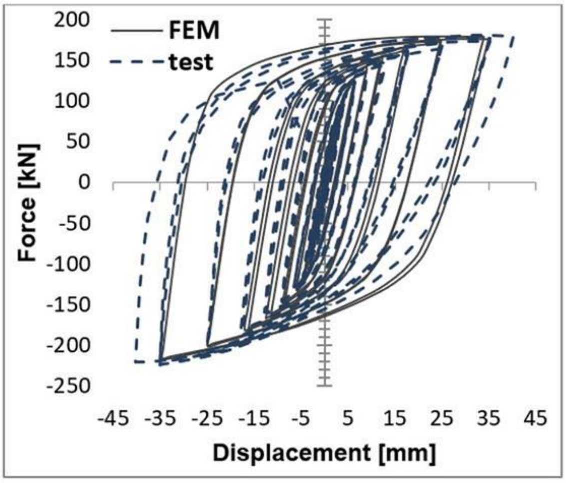

(b) NECSD.2

Fig. 14 Load–displacement curve tests versus FEA results for: (a) NECSD.1; (b) NECSD.2

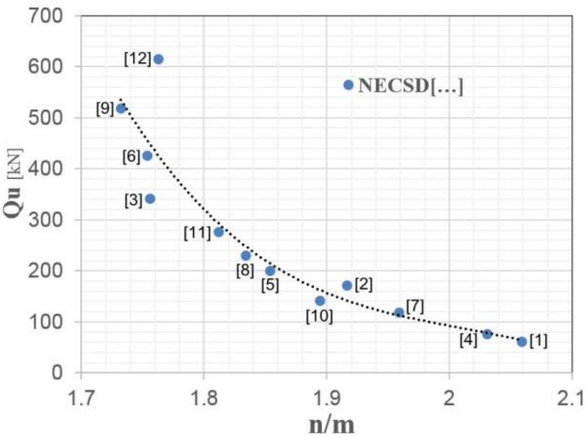

Fig. 15 The capacity of the models regarding to the n/m ratio

curvature, while in the pressure curvature, exists a steep slope in non-linear curvature with a fewer capacity. Some prominent parameter for comparing the ratio of the experimental /numerical models are tabulated in Table 4.

By matching the numerical hysteretic loops with the test, a difference area has seen in the closed area 'A_h' between the loops of the numerical and experimental models. This value in numerical loops is about 5% higher than the experimental loops. Accordingly, this value is reduced from the numerical 'A_h' data to calculate the damping ratio for all models in Table 3.

5. Parametric study and formulation

To assess the hysteretic behavior of the NECSD, some mechanical characteristics in relationship with overall capacity, stiffness, and damping ratio is discussed in this section. According to Tables 2, Fig. 15 is plotted for the capacity of the models concerning 'n/m' ratio. As observed in this figure, there exists a non-linear relationship between the overall capacity of the models and the tensile/compressive capacity ratio. The 'n/m' ratio shows the state of symmetry in the hysteretic loops; therefore, the hysteretic loops with a higher 'n/m' value tend to be more asymmetric. As shown in Fig. 15, the models with lower capacity have higher 'n/m', that means, these models tend to be more asymmetric in hysteretic loops.

This event is also predictable for the stiffness in relationship to 'st/sc' ratio. As observed in Fig. 16, an

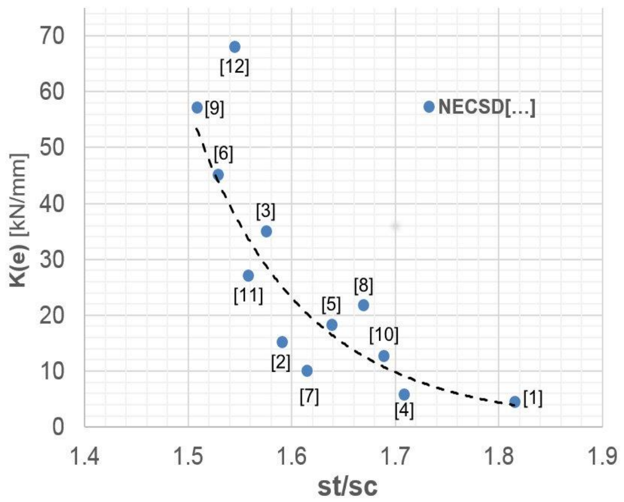

Fig. 16 The stiffness of the models regarding to the t/c ratio

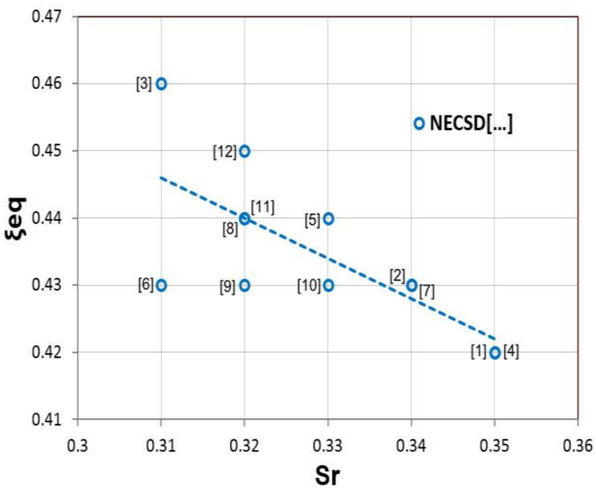

Fig. 17 Damping ratio versus effective/elastic stiffness

increase in the overall stiffness of the device, decreases the tensile/compressive ratio.

A comparison for the damping ratio to effective/elastic stiffness value: 'Sr', is shown in Fig. 17. In the NECSD models, by increasing 'Sr', the damping ratios decrease. The damping ratio increases in the hysteretic loop with a huge area, therefore by increasing the 'Sr', hysteretic loops became a slimmer body with a smaller area. In fact, for NECSD models with higher damping ratios, the curve slope in the linear state suddenly jumps to the non-linear state. This jumping causes obesity in hysteretic loops.

Based on the effective stiffness, a diagram is plotted in Fig. 18 to estimate the maximum plastic displacement: 'Dt'. As shown in this diagram, the maximum plastic displacement cannot be less than a definite minimum value. This minimum value 'Dt' is about 30 mm for NECSD models; therefore, the NECSDs with less effective stiffness could be more flexible at the plastic range.

For comparison, some of the essential parameters are listed in Table 5 for applying some of the prominent yield dampers. It could be concluded that the NECSD is a low-cost device which could easily installed at the structures

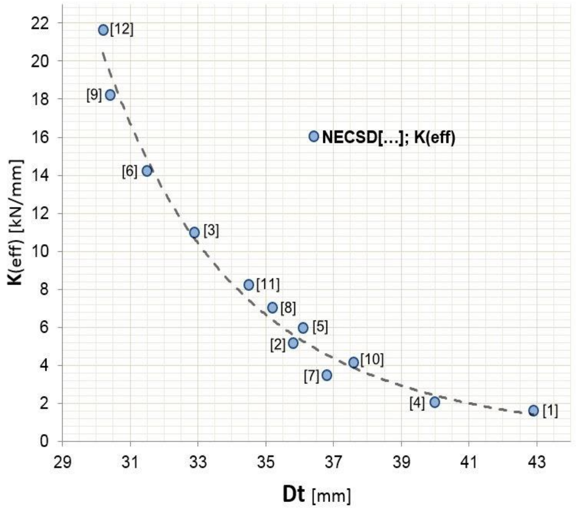

Fig. 18 Maximum plastic displacement versus effective stiffness

without using the gusset plate with an appropriate viscos damping ratio.

5.1 Design approach to estimation mechanical property of the NECSD:

Hysteretic dampers, as supplemental devices, improve the performance of the structures by dissipating a significant portion of the input seismic energy and providing an added damping ratio more than inherent damping in structures. The entire system of a frame with a hysteretic damper may be assumed as two springs. Based on the summation of two series springs, the effective stiffness of a frame with damper '$K_{a,eff}$' can be calculated by the following equation

$$\frac{1}{K_{a,eff}} = \frac{1}{K_b} + \frac{1}{K_d} \qquad \rightarrow \quad K_{a,eff} = \frac{K_d}{1 + \frac{1}{\left({K_b}/{K_d}\right)}} \tag{5}$$

where K_b and K_d are the brace stiffness and the damper stiffness, respectively. According to Eq. (5), the value of the $\left({K_b}/{K_d}\right)$ is important to damped systems behavior. By increasing the value of the$\left({K_b}/{K_d}\right)$, $K_{a,eff}$ approaches K_d; however, it is neither practical nor economical to increase the parameter excessively. Xia and Hanson (1992) suggested $\left({K_b}/{K_d}\right)$values greater than 2, considering both damper system performance and cost of bracing members. However, in this study for the design of brace, corresponding to NECSD, the stiffness of the brace is suggested more than two times of obtained stiffness of NECSDs. Therefore, for a primary estimating of mechanical property of the NECSD, according to obtained mechanical characteristics from FEA result, Eqs. (6-8) corresponding to the thickness of cylindrical shells are proposed to yield force [kN], elastic stiffness [kN/mm], and effective stiffness [kN/mm]

Table 5 Parameters in the application of yield dampers

Parameter	Damper type						
	NECSD 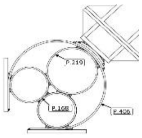	PD[a] 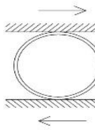	DPD[b] 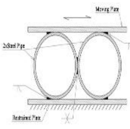	CPD[c] 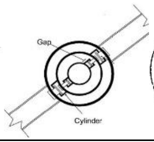	TADAS[d] 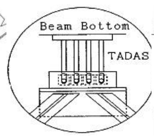	SD[e] 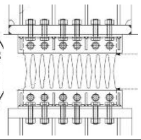	SWP[f] 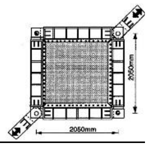
Construction cost	Very low	Very low	Very low	Middle	Difficult	Low	Middle
Installation method	Easy	Easy	Easy	Middle	Difficult	Middle	Difficult
Mechanism to yiel d	MLP[g]	SLP[h]	SLP	MLP	MLP	SLP	N/A[k]
Stability	High	Middle	Middle	Middle	High	Low	Low
Equivalent viscos damping ratio	43%	40%	30-36%	36-45%	40%	30-45%	N/A
Suitable for rise o f building	Mid-rise	Low-rise	Low-rise	Mid-rise	Mid-rise	Low-rise	Mid-rise
Height (mm)	406	114-140	110-140	406-610	304	162	2050
Mass (kg)	13-32	5-12	7-17	26-64	70-100	5-17	50-150

[a] Pipe Damper (Maleki and Bagheri, 2010),; [b] Dual Pipe Damper (Maleki and Mahjoubi, 2013); [c] Concentric Pipe D amper (Cheraghi and Zahrai, 2016); [d] Triangular-plate Added Damping And Stiffness (Tsai *et al.* 1993); [e] Slit Damp er (Ricky and Faris, 2008); [f] Shear Wall Panel (Nakagawa *et al.* 1996); [g] Multi-Load Path; [h] Single-Load Path; [k] No t Available; The values extracted from the corresponding reference; some of values calculated by the authors

$$Q_y = 29.36\ t_{p.406} + 2.86\ t_{p.219} - 1.43\ t_{p.168} - 190.3 \quad (6)$$

$$K_e = 4.96\ t_{p.406} + 3.13\ t_{p.219} - 3.71\ t_{p.168} - 36.19 \quad (7)$$

$$K_{eff} = 1.55\ t_{p.406} + 1.07\ t_{p.219} - 1.23\ t_{p.168} - 11.22 \quad (8)$$

where, $\boldsymbol{t_{p.(.)}}$, is the value of thickness [mm], and the diameters of cylindrical shells are related to their indexes.

To estimate the other mechanical properties of the proposed damper concerning to the three last equations, the following Eqs. (9-10) by fit curve from previously graphs, are proposed to equivalent viscous damping ratio and maximum plastic deformation [mm] corresponding to elastic stiffness/effective stiffness and effective stiffness, respectively.

$$\xi = -0.6(S_r) + 0.63 \quad (9)$$

$$D_t = \ln\left(\frac{11417}{K_{eff}}\right)/0.21 \quad (10)$$

6. Conclusions

In this study, a novel steel energy dissipating device by cylindrical shell structure was proposed. Applying the nested cylindrical shells structure in the configuration of this damper with a complex combination of non-linear springs in series and parallel form could be enhanced the performance and stability of the device. This configuration, as shown in an experimental specimen, could make a multi-load path mechanism to fail of components, that means, if a member fails during a loading process, the overall function of the system will not be disturbed completely. The following issues briefing in the mechanical behavior of this damper:

- Numerical models were applied to calculate the mechanical characteristics of the proposed damper, a wide range of mechanical characteristics were obtained by various thickness of the cylindrical shells (pipes). According to the results, the NECSD could be an appropriate choice for low to mid-rise buildings.
- Two full-scale prototypes corresponding to the dimensions of the FE models were built for verifying the numerical results. This verification was applied to all of the numerical models. The results of the FEAs, corresponding to the experimental data, indicate a stable hysteretic behavior under quasi-static conditions.
- A high damping ratio was obtained for NECSD. The 43% is a proper damping ratio for an energy dissipation device without resorting to the complicated and expensive energy dissipation device.
- The device with lower capacity had more asymmetric behavior in hysteretic loops. Besides, devices with thin cylindrical shells were more flexible, while devices with thick cylindrical shells, by symmetrical shape in hysteretic loops, were more capacious.

References

ABAQUS Finite Element Analysis Program (2013), "Version 6.13-1", User's Manual.

Abbasnia, R., Vetr, M.G., Ahmadi, R. and Kafi, M.A. (2008), "Experimental and analytical investigation on the steel ring ductility", *Sharif J. Sci. Technol.*, **52**, 41-48.

Andalib, Z., Kafi, M.A., Ali Kheyroddin, A., Bazzaz, M. and Momenzadeh, S.B. (2018), "Numerical evaluation of ductility and energy absorption of steel rings constructed from plates", *Eng. Struct.*, **169**, 94-106. https://doi.org/10.1016/j.engstruct.2018.05.034.

APL Specification 5L (2000), "American Petroleum Institute, USA.

ATC-24 (1992), “Guidelines for seismic testing of components of steel structures”, Applied Technology Council (ATC), Washington D.C., U.S.A.

Bergman, D.M. and Goel, S.C. (1987), “Evaluation of cyclic testing of steel plate devices for added damping and stiffness”, Report No. UMCE87-10. Ann Arbor (MI, USA): The University of Michigan, U.S.A.

Castaldo, P. (2014), “Integrated Seismic Design of Structure and Control Systems”, Springer, Berlin/Heidelberg, Germany.

Cheraghi, A and Zahrai, S.M. (2016), “Innovative multi-level control system with concentric pipes to reduce seismic response of braced steel frames”, *J. Constr. Steel Res*., **127**, 120-137. https://doi.org/10.1016/j.jcsr.2016.07.024.

Chopra, A.K. (1995), “Dynamics of structures: theory and applications to earthquake engineering”, Englewood Cliffs (NJ), U.S.A.

Deng, K., Pan, P., Su, Y. and Xue, Y. (2015), “Shape optimization of U-shaped damper for improving its bi-directional performance under cyclic loading”, *Eng. Struct*., **93**, 27-35. https://doi.org/10.1016/j.engstruct.2015.03.006.

FEMA 356 (2000), “Prestandard and commentary for the seismic rehabilitation of buildings”, Federal Emergency Management Agency (FEMA), Washington D.C., U.S.A.

FEMA 461 (2007), “Interim protocols for determining seismic performance characteristics of structural and nonstructural components”, Federal Emergency Management Agency, Washington D.C., U.S.A.

GOST (ГОСТ) 8733 (1976), “Seamless cold and warm deformed pipes”, GOST Standards of the Russian Federation, Russia.

Kim, J., Kim, M. and Nour Eldin, M. (2017), “Optimal distribution of steel plate slit dampers for seismic retrofit of structures”, *Steel Comp. Struct*., **4**, 473-484. https://doi.org/10.12989/scs.2017.25.4.473.

Liang, Z., Lee, G.C., Dargush, G.F. and Song, J. (2011), “Structural Damping Applications in Seismic Response Modification”, CRC Press, Boca Raton, Florida, U.S.A.

Maleki, S. and Bagheri, S. (2010), “Pipe damper, Part I: Experimental and analytical study”, *J. Constr. Steel Res*., **66**, 1088-1095. https://doi.org/10.1016/j.jcsr.2010.03.010.

Maleki, S. and Mahjoubi, S. (2013), “Dual-pipe damper”, *J. Constr. Steel Res*, **85**, 81-91. https://doi.org/10.1016/j.jcsr.2013.03.004.

Nakagawa, S., Kihara, H., Torii, S., Nakata, Y., Fukuda, K., Iwata, M. and Fujisawa, K. (1996), “Hysteretic behavior of low yield strength steel panel shear wall”, *11th World Conference on Earthquake Engineering*, Mexico, 171-178.

Plevris, V., Kremmyda, G. and Fahjan, Y. (2017), “Performance-based seismic design of concrete structures and infrastructures”, IGI Global, U.S.A.

Priestley, M.J.N., Calvi, G.M. and Kowalsky, M.J. (2007), “Displacement based seismic design of structures”, IUSS Press, Italy.

Ricky, W.K.C. and Faris, A. (2008), “Experimental study of steel slit damper for passive energy dissipation”, *Eng. Struct*., **30**, 1058-1066. https://doi.org/10.1016/j.engstruct.2007.07.005.

Soong, T.T. and Dargush, G.F. (1997), “Passive energy dissipation system in structural engineering”, John Wiley and Sons, New York, U.S.A.

Soong, T.T. and Spencer Jr, B.F. (2002), “Supplemental energy dissipation: state-of-the-art and state of-the-practice”, *Eng. Struct*., **24**(3), 243-259. https://doi.org/10.1016/S0141-0296(01)00092-X.

Suzuki, K. and Watanabe, A. (2000), “Experimental study of U-shaped steel damper”, Summary of technical papers of annual meeting, Architectural Institute of Japan, B-2.

Tagawa, H., Yamanishi, T., Takaki, A. and Chan, R.W.K., (2016), “Cyclic behavior of seesaw energy dissipation system with steel slit dampers”, *J. Constr. Steel Res*., **117**, 24-34. https://doi.org/10.1016/j.jcsr.2015.09.014.

Tsai, K., Chen, H., Hong, C. and Su, Y. (1993), “Design of steel triangular plate energy absorbers for seismic-resistant construction”, *Earthq. Spectra,* **9**(3), 505-528. https://doi.org/10.1193/1.1585727.

Ventsel, E. and Krauthammer, T. (2001), “Thin Plates and Shells: Theory, Analysis, and Applications”, Marcel Dekker, New York, U.S.A.

Vodenitcharova, T. and Ansourian, P. (1998), “Hydrostatic, wind and non-uniform lateral pressure solutions for containment vessels”, *Thin-Walled Struct*., **31**, 221-236. https://doi.org/10.1016/S0263-8231(98)00008-1.

Xia, C. Hanson, R. (1992), “Influence of ADAS element parameters on building seismic response”, *J. Struct. Eng*. **118**(7) 1903-1918. https://doi.org/10.1061/(ASCE)0733-9445(1992)118:7(1903).

Zahrai, S.M. and Cheraghi, A. (2017), “Improving cyclic behavior of multi-level pipe damper using infill or slit diaphragm inside inner pipe”, *Struct. Eng. Mech*., **64**(2), 195-204. https://doi.org/10.12989/sem.2017.64.2.195.

Zhang, C., Aoki, T., Zhang, Q. and Wu, M. (2015), “The performance of low-yield-strength steel shear-panel damper with without buckling”, *Mat. Struct*., **48**, 1233-1242. https://doi.org/10.1617/s11527-013-0228-9.

AT